[10] G. L. Stüber, *Principles of Mobile Communication*. Berlin, Germany: Springer-Verlag, 2011.
[11] A. Abdi and M. Kaveh, "K distribution: An appropriate substitute for rayleigh-lognormal distribution in fading-shadowing wireless channels," *Electron. Lett.*, vol. 34, no. 9, pp. 851–852, Apr. 1998.
[12] P. M. Shankar, "Error rates in generalized fading channels," *Wireless Pers. Commun.*, vol. 28, no. 3, pp. 233–238, Feb. 2004.
[13] M. Uysal, J. Li, and M. Yu, "Error rate performance analysis of coded free-space optical links over gamma-gamma atmospheric turbulence channels," *IEEE Trans. Wireless Commun.*, vol. 5, no. 6, pp. 1229–1233, Jun. 2006.
[14] A. Laourine, M. S. Alouini, S. Affes, and A. Stephenne, "On the performance analysis of composite multipath/shadowing channels using the $\mathcal{G}$-distribution," *IEEE Trans. Commun.*, vol. 57, no. 4, pp. 1162–1170, Apr. 2009.
[15] J. Cao, L.-L. Yang, and Z. Zhong, "Performance analysis of multihop wireless links over generalized-K fading channels," *IEEE Trans. Veh. Technol.*, vol. 61, no. 4, pp. 1590–1598, May. 2012.
[16] A. Abdi and M. Kaveh, "Comparison of DPSK and MSK bit error rates for k and rayleigh-lognormal fading distributions," *IEEE Commun. Lett.*, vol. 4, no. 4, pp. 122–124, Apr. 2000.
[17] P. S. Bithas, P. T. Mathiopoulos, and S. A. Kotsopoulos, "Diversity reception over generalized-K fading channels," *IEEE Trans. Wireless Commun.*, vol. 6, no. 12, pp. 4238–4243, Dec. 2007.
[18] P. M. Shankar, "Performance analysis of diversity combining algorithms in shadowed fading channels," *Wireless Pers. Commun.*, vol. 37, no. 1/2, pp. 61–72, Feb. 2006.
[19] C. Zhu, J. Mietzner, and R. Schober, "On the performance of non-coherent transmission schemes with equal-gain combining in generalized-fading," *IEEE Trans. Wireless Commun.*, vol. 9, no. 4, pp. 1337–1349, Apr. 2010.
[20] K. P. Peppas, "Performance evaluation of triple-branch GSC diversity receivers over generalized-K fading channels," *IEEE Commun. Lett.*, vol. 13, no. 11, pp. 829–831, Nov. 2009.
[21] K. P. Peppas, "Accurate closed-form approximations to generalised-K sum distributions and applications in the performance analysis of equal-gain combining receivers," *IET Commun.*, vol. 5, no. 7, pp. 982–989, Jul. 2011.
[22] I. Gradshteyn and I. Ryzhik, *Table of Integrals, Series and Products*, 7th ed. San Diego, CA, USA: Academic, 2007.
[23] P. S. Bithas, N. C. Sagias, P. T. Mathiopoulos, G. K. Karagiannidis, and A. A. Rontogiannis, "On the performance analysis of digital communications over generalized-K fading channels," *IEEE Commun. Lett.*, vol. 10, no. 5, pp. 353–355, Jan. 2006.
[24] N. D. Chatzidiamantis, G. K. Karagiannidis, and D. S. Michalopoulos, "On the distribution of the sum of gamma-gamma variates and application in MIMO optical wireless systems," in *Proc. IEEE GLOBECOM*, Honolulu, HI, USA, Nov. 2009, pp. 1–6.
[25] N. D. Chatzidiamantis and G. K. Karagiannidis, "On the distribution of the sum of gamma-gamma variates and applications in RF and optical wireless communications," *IEEE Trans. Commun.*, vol. 59, no. 5, pp. 1298–1308, May 2011.
[26] S. Al-Ahmadi and H. Yanikomeroglu, "On the approximation of the PDF of the sum of independent generalized-K RVs by another generalized-K PDF with applications to distributed antenna systems," in *Proc. IEEE WCNC*, Sydney, NSW, Australia, Apr. 2010, pp. 1–6.
[27] S. Al-Ahmadi and H. Yanikomeroglu, "The ergodic and outage capacities of distributed antenna systems in generalized-K fading channels," in *Proc. IEEE PIMRC*, Istanbul, Turkey, Sep. 2010, pp. 662–666.
[28] A. P. Prudnikov, Y. A. Brychkov, and O. I. Marichev, *Integrals and Series: Vol. 3: More Special Functions*. New York, NY, USA: CRC, 1992.
[29] V. S. Adamchik and O. I. Marichev, "The algorithm for calculating integrals of hypergeometric type functions and its realization in REDUCE system," in *Proc. IEEE ISSAC*, Tokyo, Japan, Aug. 1990, pp. 212–224.
[30] M. Bloch, J. Barros, M. R. Rodrigues, and S. W. McLaughlin, "Wireless information-theoretic security," *IEEE Trans. Inf. Theory*, vol. 54, no. 6, pp. 2515–2534, Jun. 2008.
[31] S. C. Gupta, "Integrals involving products of G-function," *Proc. Nat. Acad. Sci.*, vol. A-39, no. II, pp. 193–200, Apr. 1969.
[32] M. Shah, "On generalizations of some results and their applications," *Collectanea Math.*, vol. 24, no. 3, pp. 249–266, Mar. 1973.
[33] "The Wolfram functions site," Wolfram, Champaign, IL, USA, 2001. [Online]. Available: http://functions.wolfram.com
[34] I. S. Ansari, S. Al-Ahmadi, F. Yilmaz, M. S. Alouini, and H. Yanikomeroglu, "A new formula for the BER of binary modulations with dual-branch selection over generalized-K composite fading channels," *IEEE Trans. Commun.*, vol. 59, no. 10, pp. 2654–2658, Oct. 2011.
[35] K. P. Peppas, "A new formula for the average bit error probability of dual-hop amplify-and-forward relaying systems over generalized shadowed fading channels," *IEEE Wireless Commun. Lett.*, vol. 1, no. 2, pp. 85–88, Apr. 2012.
[36] E. Zedini, I. S. Ansari, and M.-S. Alouini, "Performance analysis of mixed nakagami-m and gamma-gamma dual-hop FSO transmission systems," *IEEE Photon. J.*, vol. 7, no. 1, pp. 1–20, Feb. 2015.
[37] H. Lei, C. Gao, Y. Guo, and G. Pan, "On physical layer security over generalized gamma fading channels," *IEEE Commun. Lett.*, vol. 19, no. 7, pp. 1257–1260, Jul. 2015.
[38] M. Springer and W. Thompson, "The distribution of products of beta, gamma and gaussian random variables," *SIAM J. Appl. Math.*, vol. 18, no. 4, pp. 721–737, Jun. 1970.

A Two-Stage Vector Perturbation Scheme for Adaptive Modulation in Downlink MU-MIMO

Ang Li, *Student Member, IEEE*, and
Christos Masouros, *Senior Member, IEEE*

***Abstract*—Conventional vector perturbation (VP) is not directly applicable to adaptive modulation, whereas other existing algorithms are suboptimal due to the reduced search dimension of perturbation vectors. In this paper, by applying a simple transformation to the conventional VP operation, the search dimension for the proposed joint VP is made equal to that of conventional VP, and therefore, the performance advantages of VP still hold in this scenario. Furthermore, to reduce the computational complexity, a joint constructive VP scheme is introduced by exploiting constructive interference to simplify the VP operation. By doing so, the sophisticated search for perturbation vectors is partially replaced by a quadratic programming problem, therefore saving significant computational complexity. Our analysis and results show that the proposed scheme offers an improved performance–complexity tradeoff compared with conventional VP approaches by means of the measurement in energy efficiency.**

***Index Terms*—Adaptive modulation, multiple-input–mulitple-output (MIMO), precoding, two-stage perturbation, vector perturbation (VP).**

I. Introduction

In recent multiple-input–multiple-output (MIMO) communication systems, precoding techniques have been widely studied, and simple forms of precoding have appeared in communication standards [1], [2]. Existing precoding approaches range from linear precoding [3] to nonlinear precoding [4]. Nonlinear vector perturbation (VP)-based

Manuscript received March 16, 2015; revised June 16, 2015 and August 20, 2015; accepted October 7, 2015. Date of publication October 9, 2015; date of current version September 15, 2016. This work was supported in part by the Royal Academy of Engineering and in part by the Engineering and Physical Sciences Research Council under Project EP/M014150/1. The review of this paper was coordinated by Prof. Y. Zhou.

The authors are with the Department of Electronic and Electrical Engineering, University College London, London WC1E 7JE, U.K. (e-mail: ang.li.14@ucl.ac.uk; chris.masouros@ieee.org).

Color versions of one or more of the figures in this paper are available online at http://ieeexplore.ieee.org.

Digital Object Identifier 10.1109/TVT.2015.2489263

precoding in [4]–[7] improves the performance of linear channel inversion precoding schemes. However, one drawback of conventional VP scheme is that it does not apply to scenarios where multiple modulation types are employed by different users due to the fact that the modulo base $\tau = 2|C|_{\max} + \Delta$ is modulation dependent, where $|C|_{\max}$ is the absolute value of the constellation symbol with the maximum magnitude, and Δ denotes the minimum Euclidean distance between constellation points. In [8], VP is combined with block-diagonalized (BD) precoding as BD-VP to enable VP technique applicable for adaptive modulation scenario. Nevertheless, due to the operation of singular value decomposition, BD-VP is computationally inefficient. To circumvent this, a low-complexity BD-VP scheme is introduced in [9], and a user-grouping VP (UG-VP) is also proposed to improve the performance of BD-VP. However, both BD-VP and UG-VP are suboptimal to conventional VP due to the reduced search dimensions.

In [10], a joint VP (JVP) algorithm is proposed that enables VP applicable to adaptive modulation scenarios without degrading the performance. By scaling the constellation of different modulation types and the corresponding channel matrix, the modulo base τ is made common for all modulation types, and therefore, a full dimension search for the perturbation vectors could be performed. However, the computational complexity of the proposed scheme in [10] is comparable with conventional VP schemes. Therefore, to reduce the complexity, in this paper, a two-stage joint constructive VP (JCVP) scheme is further introduced. In the first stage, the search for the perturbation vectors is exclusively limited for users applying quadratic-amplitude modulation (QAM) modulation, whereas in the second stage, the constructive VP (CVP) [11] is performed for users applying phase-shift keying (PSK) modulation, where the search space is limited to the areas that are constructive to the transmit symbols. These are the areas where the perturbation vectors can increase the distances to the decision thresholds of the constellation and therefore can increase the detection performance. Moreover, as the constructive perturbation vectors need not be removed because they will benefit the symbol detection, the perturbation vectors need not be integers. Therefore, instead of using the sophisticated sphere encoding technique, a quadratic programming method could be applied, thus saving much computational complexity, particularly when the search dimension is large.

For reasons of clarity, we summarize the contributions of this paper as follows.

1) We propose a reduced-complexity two-stage VP scheme for adaptive modulation scenarios.
2) We derive the performance of the proposed scheme analytically in the presence of imperfect channel state information (CSI).
3) We characterize the performance–complexity tradeoff for the proposed and conventional schemes by introducing an energy efficiency metric.

Notation: $E(\cdot)$, $(\cdot)^T$, $(\cdot)^H$, $(\cdot)^{-1}$, and $(\cdot)^\dagger$ denote expectation, transpose, conjugate transpose, inverse, and Moore–Penrose inverse, respectively. $\|\cdot\|$ denotes the Frobenius norm, I_n is the $n \times n$ identity matrix, and $\mathbf{0}$ denotes zero matrix or vector. $\mathbf{R}^{n\times n}$ represents an $n \times n$ matrix in the real set, and $\mathbf{CZ}^n$ represents $n \times 1$ vectors in the complex integer set.

II. System Model and Conventional Vector Perturbation

A. MU-MIMO Channel Model

A multiuser multistream MIMO downlink system is considered, where the base station communicates with K users simultaneously. It is assumed that the base station is equipped with N_t antennas with each user k equipped with $n_k \geq 1$ antennas. The total number of receive antennas is therefore defined as $N_r = \sum_{k=1}^{K} n_k$, with $N_r \leq N_t$. A flat-fading channel is assumed and modeled by the $n_k \times N_t$ channel matrix $\mathbf{H}_k$ for user k, and the channel matrix from the base station to all users can be expressed as $\mathbf{H} = [\mathbf{H}_1^T, \mathbf{H}_2^T, \ldots, \mathbf{H}_K^T]^T$. Then, the received signal at the kth user is

$$\mathbf{y}_k = \mathbf{H}_k \mathbf{x}_k + \mathbf{H}_k \sum_{i=1, i\neq k}^{K} \mathbf{x}_i + \mathbf{w}_k \tag{1}$$

where $\mathbf{x}_k$ is the precoded signal to transmit, and $\mathbf{w}_k$ is the additive complex Gaussian noise vector with zero mean and unit variance.

B. Vector Perturbation Precoding

VP precoding employs a channel inversion to form the precoding matrix and then applies a perturbation on the transmitted symbols. For each user k, the transmitted signal is then given as

$$\mathbf{x}_k = \sqrt{\frac{P}{\beta}} \mathbf{F}_k \left(\mathbf{s}_k + \tau \mathbf{l}_k^*\right) \tag{2}$$

where $\mathbf{F}_k$ is the precoding matrix of the kth user, and $\mathbf{s}_k$ denotes the data symbols of the kth user. $\beta = \|\mathbf{F} \cdot (\mathbf{s} + \tau \mathbf{l})\|^2$ denotes the transmit power scaling factor so that $E(\|\mathbf{x}\|^2) = P$, where $\mathbf{s} = [\mathbf{s}_1^T, \mathbf{s}_2^T, \ldots, \mathbf{s}_K^T]^T$, and $\mathbf{x} = [\mathbf{x}_1^T, \mathbf{x}_2^T, \ldots, \mathbf{x}_K^T]^T$. $\mathbf{l}^* \in \mathbf{CZ}^{N_t}$ is the perturbation vector. Usually in VP, the precoding matrix could be in the form of channel inversion, and channel inversion can be viewed as a special case where $\mathbf{l}^* = \mathbf{0}$. The received signal of VP for user k after the channel can be calculated as

$$\mathbf{y}_k = \sqrt{\frac{P}{\beta}} \left(\mathbf{s}_k + \tau \mathbf{l}_k^*\right) + \mathbf{w}_k. \tag{3}$$

At the receiver, the signal is first scaled back to eliminate the effect of the transmit scaling factor and then fed to a modulo operator to remove the perturbation vector [4]. Ignoring the effect of modulo loss, the output symbols of modulo operation can be expressed as

$$\begin{aligned} \mathbf{r}_k &= \mathrm{mod}_\tau \left[\sqrt{\frac{\beta}{P}} \mathbf{y}_k\right] = \mathrm{mod}_\tau \left[\mathbf{s}_k + \tau \mathbf{l}_k^* + \sqrt{\frac{\beta}{P}} \mathbf{w}_k\right] \\ &= \mathbf{s}_k + \mathbf{n}_k \end{aligned} \tag{4}$$

where

$$\mathrm{mod}_\tau[x] = f_\tau\left(\Re(x)\right) + j \cdot f_\tau\left(\Im(x)\right) \tag{5}$$

$$f_\tau(x) = x - \left\lfloor \frac{x + \tau/2}{\tau} \right\rfloor \cdot \tau \tag{6}$$

$\mathbf{n}_k$ denotes the noise for user k after the modulo operation.

III. Proposed Two-Stage Joint Constructive Vector Perturbation

A. Joint Vector Perturbation

In conventional VP algorithm, the perturbation vector $\mathbf{l}^{\mathrm{opt}}$ is searched over N_r dimensions to minimize the total transmit power. However, due to the fact that different modulations have different values of τ, conventional VP cannot be directly applied to scenarios where users employ multiple modulation types. To keep the performance advantage of conventional VP, we employ a joint perturbation technique that retains the search dimensions as N_r. Without loss of generality, we assume that there are multiple modulation

types applied, which are denoted by $\mathcal{A}, \mathcal{B}, \mathcal{C}, \ldots, \mathcal{M}$. For modulation type i, the total number of symbols applying this kind of modulation is denoted by N_i, and $\sum_{i=\mathcal{A}}^{\mathcal{M}} N_i = N_r$. For conventional VP, $\mathbf{l}^{\text{opt}} = \arg\min_{\mathbf{l}\in\mathbf{Z}^{N_r}} \|\mathbf{F}(\mathbf{s}+\tau\mathbf{l})\|^2$, where $\mathbf{F}$ is the precoding matrix. Rewrite $\mathbf{F}=[\mathbf{F}_{\mathcal{A}}, \mathbf{F}_{\mathcal{B}}, \ldots, \mathbf{F}_{\mathcal{M}}]$, $\mathbf{s}+\tau\mathbf{l}=[(\mathbf{s}_{\mathcal{A}}+\tau_{\mathcal{A}}\mathbf{l}_{\mathcal{A}})^T, (\mathbf{s}_{\mathcal{B}}+\tau_{\mathcal{B}}\mathbf{l}_{\mathcal{B}})^T, \ldots, (\mathbf{s}_{\mathcal{M}}+\tau_{\mathcal{M}}\mathbf{l}_{\mathcal{M}})^T]^T$, where $\mathbf{s}_i$ denotes the symbols from the constellation of modulation type i, and $\mathbf{F}_i$ is the corresponding precoding matrix. Then, we can reformulate the transmit signal norm as

$$\begin{aligned}\|\mathbf{F}(\mathbf{s}+\tau\mathbf{l})\|^2 &= \|[\mathbf{F}_{\mathcal{A}}, \mathbf{F}_{\mathcal{B}}, \ldots, \mathbf{F}_{\mathcal{M}}]\cdot(\mathbf{s}+\tau\mathbf{l})\|^2 \\ &= \left\|\sum_{i=\mathcal{A}}^{\mathcal{M}} \frac{\tau_i}{\tau_0}\cdot\frac{\tau_0}{\tau_i}\mathbf{F}_i(\mathbf{s}_i+\tau_i\mathbf{l}_i)\right\|^2 \\ &= \left\|\sum_{i=\mathcal{A}}^{\mathcal{M}} \frac{\tau_i}{\tau_0}\mathbf{F}_i\left(\frac{\tau_0}{\tau_i}\mathbf{s}_i+\tau_0\mathbf{l}_i\right)\right\|^2 \end{aligned} \tag{7}$$

where $\mathbf{l}_i$ is the perturbation vector for modulation type i, and τ_0 denotes the modulo base to be used. Based on the derivation earlier, it is worth noting that there is no special restriction for the value of τ_0 as when the symbols are scaled, the corresponding channel is also scaled accordingly. By defining $\mathbf{G} = [\{\tau_{\mathcal{A}}/\tau_0\}\mathbf{F}_{\mathcal{A}}, \ldots, \{\tau_{\mathcal{M}}/\tau_0\}\mathbf{F}_{\mathcal{M}}]$ and $\mathbf{t} = [\{\tau_0/\tau_{\mathcal{A}}\}s_{\mathcal{A}}^T, \ldots, \{\tau_0/\tau_{\mathcal{M}}\}s_{\mathcal{M}}^T]^T$, (7) can be transformed into

$$\|\mathbf{F}(\mathbf{s}+\tau\mathbf{l})\|^2 = \|\mathbf{G}(\mathbf{t}+\tau_0\mathbf{l})\|^2. \tag{8}$$

With this transformation, the search for the perturbation vectors in adaptive modulation scenario is kept the same as conventional VP scheme. Intuitively, this algorithm functions as follows: By scaling the constellation of the modulation and the corresponding channel matrix, different modulation types have the same value of τ with no any change in the value of the signal norm so that the VP could be performed jointly.

B. Complexity Reduction by Joint Constructive Vector Perturbation

Although JVP preserves the performance benefits of conventional VP, it also preserves the high computational complexity of conventional VP. To reduce the complexity, the CVP first introduced in [11] is applied in the adaptive modulation scenario. By limiting the search space for the perturbation vectors to the constructive areas where the symbols have increased distances to the decision thresholds of the constellation, the perturbation vectors for CVP at the receivers need not be removed, and therefore need not be integers. As conventional CVP is not applicable to our scheme, we propose a modification in the following. For notational simplicity, let us first decompose the channel and information symbols into real and imaginary parts as

$$\hat{\mathbf{H}} = \begin{bmatrix} \Re(\mathbf{H}) & -\Im(\mathbf{H}) \\ \Im(\mathbf{H}) & \Re(\mathbf{H}) \end{bmatrix} \tag{9}$$

$$\hat{\mathbf{s}} = \begin{bmatrix} \Re(\mathbf{s})^T & \Im(\mathbf{s})^T \end{bmatrix}^T. \tag{10}$$

Then, the transmit signal is modified by applying a diagonal scaling matrix $\mathbf{\Theta} \in \mathbf{R}^{2N_t\times 2N_t}$ and can be formulated as

$$\hat{\mathbf{x}} = \sqrt{\frac{P}{\beta}}\mathbf{F}(\mathbf{\Theta}\hat{\boldsymbol{s}}). \tag{11}$$

In this case, the scaling factor is obtained as

$$\beta = \|\mathbf{F}(\mathbf{\Theta}\hat{\boldsymbol{s}})\|^2. \tag{12}$$

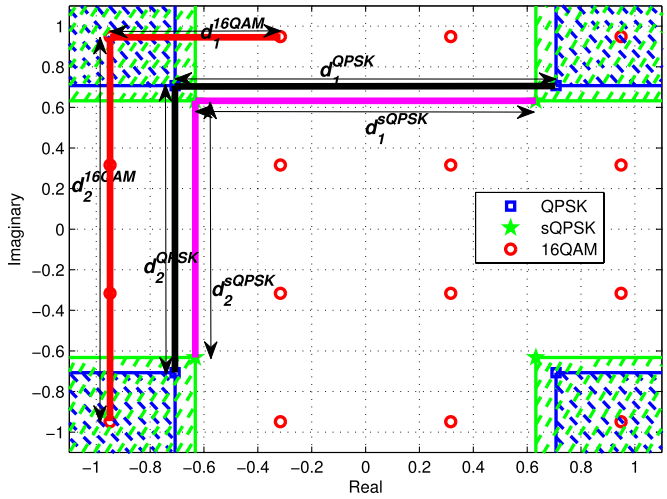

Fig. 1. Constructive areas for QPSK and sQPSK in the normalized constellation.

It is well established in the literature that the computational complexity of conventional VP grows exponentially with the increase in search dimension, whereas it is shown that the complexity of CVP reduces to the polynomial complexity [11]. To preserve the complexity advantage of CVP in the adaptive modulation scenario, a two-stage JCVP scheme is then introduced. By using the concept of selective perturbation, only the symbols from QAM constellations are perturbed in the first stage, followed by a partial CVP scheme for the symbols from PSK constellations. To be specific, in the first stage, the optimization for the perturbation vector of (8) is modified as

$$\mathbf{l}^* = \arg\min \left\|\bar{\mathbf{G}}\left(\bar{\mathbf{t}} + \tau_0\begin{bmatrix}\mathbf{0}_{N_t-L}\\ \mathbf{l}_L\end{bmatrix}\right)\right\|^2 \tag{13}$$

where L denotes the total number of symbols from QAM constellations; and $\bar{\mathbf{t}}$ and $\bar{\mathbf{G}}$ denote the appropriate reordering of the transmit symbols and the corresponding matrix $\mathbf{G}$ after performing JVP, respectively. Rewriting $\bar{\mathbf{G}} = [\bar{\mathbf{G}}_{N_t-L}, \bar{\mathbf{G}}_L]$, (13) can be further expressed as

$$\mathbf{l}^* = \arg\min \left\|\bar{\mathbf{G}}\bar{\mathbf{t}} + \tau_0\bar{\mathbf{G}}_L\mathbf{l}_L\right\|^2. \tag{14}$$

Then, (14) is an L-dimensional VP problem and can be solved by standard sphere search techniques.

In the second stage, a partial CVP is applied for symbols from PSK modulations to minimize the scaling factor. As aforementioned, we exploit the illustration of JVP and the constructive interference, as shown in Fig. 1, where we assume that τ_0 is chosen as $\tau_{16\text{QAM}}$ for simplicity. According to the definition of τ, the length of the fold lines $\tau_{16\text{QAM}} = d_1^{16\text{QAM}} + d_2^{16\text{QAM}}$ and $\tau_{\text{QPSK}} = d_1^{\text{QPSK}} + d_2^{\text{QPSK}}$ denotes the value of the modulo bases for 16quadrature amplitude modulation (QAM) and quadrature phase shift keying (QPSK), respectively. We scale the constellation of QPSK by $\tau_{16\text{QAM}}/\tau_{\text{QPSK}}$ such that $\tau_{16\text{QAM}}/\tau_{\text{sQPSK}} = (d_1^{16\text{QAM}} + d_2^{16\text{QAM}})/(d_1^{\text{sQPSK}} + d_2^{\text{sQPSK}}) = 1$, and therefore, JVP could be performed. Moreover, the blue zone denotes the initial constructive area of QPSK, whereas the green zone denotes the constructive area of sQPSK, as defined in [11]. Denote $\bar{\mathbf{u}} = \bar{\mathbf{t}} + \tau_0\begin{bmatrix}\mathbf{0}_{N_t-L}\\ \mathbf{l}_L^*\end{bmatrix} = [\mathbf{u}_{N_t-L}^T, \mathbf{u}_L^T]^T$, and $\mathbf{u}_{N_t-L}^T$ are the symbols to be optimized in this stage. Then, following a similar step of CVP, a diagonal scaling matrix $\bar{\mathbf{\Theta}} \in \mathbf{R}^{2N_t\times 2N_t}$ is applied. Noticing that the scaling is only

applied for symbols from PSK constellations, the scaling factor can be formulated as

$$\beta = \left\| \hat{\bar{\mathbf{G}}} (\bar{\mathbf{\Theta}} \hat{\bar{\mathbf{u}}}) \right\|^2 \tag{15}$$

where $\hat{\bar{\mathbf{G}}}$ and $\hat{\bar{\mathbf{u}}}$ are obtained by expanding the real and imaginary parts of $\bar{\mathbf{G}}$ and $\bar{\mathbf{u}}$. Then, by defining $\bar{\boldsymbol{\theta}} = \mathrm{diag}(\bar{\mathbf{\Theta}})$, $\hat{\bar{\mathbf{U}}} = \mathrm{diag}(\hat{\bar{\mathbf{u}}})$, $\mathbf{R}^{1/2} = \hat{\bar{\mathbf{G}}} \hat{\bar{\mathbf{U}}}$, and, with some rearrangements, a simplified quadratic programming can be obtained as

$$\begin{aligned} \bar{\boldsymbol{\theta}} = \arg\min_{\bar{\boldsymbol{\theta}}} \quad & \bar{\boldsymbol{\theta}}^T \mathbf{R} \bar{\boldsymbol{\theta}} \\ \text{s.t.} \quad & \bar{\boldsymbol{\theta}}_{1:N_t-L} \geq 1, \bar{\boldsymbol{\theta}}_{N_t+1:2N_t-L} \geq 1 \\ & \bar{\boldsymbol{\theta}}_{N_t-L+1:N_t} = 1, \bar{\boldsymbol{\theta}}_{2N_t-L+1:2N_t} = 1 \end{aligned} \tag{16}$$

where $\bar{\theta}_i$ is the ith diagonal element of $\bar{\mathbf{\Theta}}$. The second line of the constraints ensures that QAM symbols are not scaled. As we already split the transmit symbols into the real and imaginary parts, we must ensure that the scaling factor of QAM symbols for both is equal to 1. In the second stage, the symbols from QAM constellations are not scaled, and this is guaranteed by setting the corresponding $\bar{\theta}$ equal to 1, as seen from (16). Finally, the transmit scaling factor is obtained as

$$\begin{aligned} \beta &= \left\| \bar{\mathbf{G}} \hat{\mathbf{\Theta}} \bar{\boldsymbol{u}} \right\|^2 = \left\| \left[\bar{\mathbf{G}}_{N_t-L}, \bar{\mathbf{G}}_L \right] \cdot \begin{bmatrix} \hat{\mathbf{\Theta}}_{N_t-L} \cdot \bar{\mathbf{t}}_{N_t-L} \\ \bar{\mathbf{t}}_L + \tau_0 \mathbf{l}_L^* \end{bmatrix} \right\|^2 \\ &= \left\| \bar{\mathbf{G}}_{N_t-L} \hat{\mathbf{\Theta}}_{N_t-L} \bar{\mathbf{t}}_{N_t-L} + \bar{\mathbf{G}}_L \cdot (\bar{\mathbf{t}}_L + \tau_0 \mathbf{l}_L^*) \right\|^2 \end{aligned} \tag{17}$$

where $\hat{\mathbf{\Theta}}$ is defined as the complex equivalent of $\bar{\mathbf{\Theta}}$.

Remark: It is natural to consider that these two steps can be performed conversely. However, it will be shown in the simulation results that applying conventional VP followed by CVP always results in a better performance for JCVP. This can be explained as follows. In the second stage, compared with conventional VP that only searches limited integers, CVP searches the entire constructive areas such that there is a higher possibility that the scaling factor is minimized.

IV. Performance Analysis in the Presence of Channel State Information Errors

Here, we present a mathematical performance analysis for JCVP in the presence of CSI errors. For analytical tractability, we focus on the case where the precoding matrix $\mathbf{F} = \mathbf{H}^\dagger$. In realistic communication systems where there exist CSI errors, we assume that the errors are inversely proportional to the transmit SNR and, therefore, can be modeled as

$$\hat{\mathbf{H}} = \mathbf{H} + \mathbf{E} \tag{18}$$

with $\mathbf{E} \sim \mathcal{C}N(0, \eta \cdot \mathbf{I}_{N_t})$, statistically independent to $\mathbf{H}$. Therefore, the channel is modeled as [12]

$$\mathbf{H} = \frac{1}{1+\eta} \cdot \hat{\mathbf{H}} + \mathbf{Q} \tag{19}$$

with $\mathbf{Q} \sim \mathcal{C}N(0, (\eta/(1+\eta)) \cdot \mathbf{I}_{N_t})$. As we assume that the system operates in TDD mode and the CSI is directly measured at the transmitter using reciprocity, η is defined as $\eta = \alpha \cdot (P/\sigma^2)^{-1}$, with α being the channel error coefficient, and P/σ^2 being the transmit SNR [11]. In this paper, we apply the constructive perturbation for PSK users while retaining the conventional perturbation operation for QAM users. Therefore, at the receiver, the received SNR for PSK users and QAM users must be calculated independently. First, the received signals of users applying PSK modulation can be expressed as

$$\begin{aligned} \mathbf{y}_{\mathrm{PSK}} &= \sqrt{\frac{P}{\beta}} \left(\frac{1}{1+\eta} \hat{\mathbf{H}} + \mathbf{Q} \right) \hat{\mathbf{H}}^\dagger \hat{\mathbf{\Theta}} \mathbf{s}_{\mathrm{PSK}} + \mathbf{w} \\ &= \frac{1}{1+\eta} \sqrt{\frac{P}{\beta}} \hat{\mathbf{\Theta}} \mathbf{s}_{\mathrm{PSK}} + \sqrt{\frac{P}{\beta}} \mathbf{Q} \hat{\mathbf{H}}^\dagger \hat{\mathbf{\Theta}} \mathbf{s}_{\mathrm{PSK}} + \mathbf{w} \end{aligned} \tag{20}$$

where $\mathbf{w}$ denotes the noise vector that consists of the noise term for each user. We then define

$$\hat{\mathbf{w}}_{\mathrm{PSK}} = \sqrt{\frac{P}{\beta}} \mathbf{Q} \hat{\mathbf{H}}^\dagger \hat{\mathbf{\Theta}} \mathbf{s}_{\mathrm{PSK}} + \mathbf{w} \tag{21}$$

as the equivalent noise term, and $\hat{\mathbf{w}}_{\mathrm{PSK}} \sim \mathcal{C}N(0, v_{\mathrm{PSK}})$, where v_{PSK} is given as [12]

$$v_{\mathrm{PSK}} = \frac{P}{\beta} \cdot \frac{\eta}{1+\eta} \cdot \beta \cdot \bar{\theta}_i^2 + \sigma^2 = \frac{\eta P \bar{\theta}_i^2}{1+\eta} + \sigma^2. \tag{22}$$

Then, the SNR of users applying PSK modulation can be calculated as

$$\gamma_i = \frac{1}{(1+\eta)^2 \beta} \cdot \frac{P \bar{\theta}_i^2}{\left(\frac{\eta P \bar{\theta}_i^2}{1+\eta} + \sigma^2 \right)} \tag{23}$$

where term $(1+\eta)^2\beta$ is due to the fact that the signals must be scaled back before demodulation.

Then, for users applying QAM modulation, by expanding (4), scaling back the signals by $(1+\eta)\sqrt{\beta/P}$, and considering the modulo operation, the received signal can be expressed as

$$\mathbf{y}_{\mathrm{QAM}} = \mathbf{s}_{\mathrm{QAM}} + \tau \mathbf{l} + (1+\eta)\, \mathbf{Q} \hat{\mathbf{H}}^\dagger \left(\mathbf{s}_{\mathrm{QAM}} + \tau \mathbf{l} \right) + (1+\eta) \sqrt{\frac{\beta}{P}} \mathbf{w} \tag{24}$$

where we define

$$\hat{\mathbf{w}}_{\mathrm{QAM}} = (1+\eta)\, \mathbf{Q} \hat{\mathbf{H}}^\dagger \left(\mathbf{s}_{\mathrm{QAM}} + \tau \mathbf{l} \right) + (1+\eta) \sqrt{\frac{\beta}{P}} \mathbf{w} \tag{25}$$

as the equivalent noise term. Based on [12], the distribution of $\hat{\mathbf{w}}_{\mathrm{QAM}}$ is conditioned on $\hat{\mathbf{H}}^\dagger$ and $\hat{\mathbf{w}}_{\mathrm{QAM}} \sim \mathcal{C}N(0, v_{\mathrm{QAM}})$, where v_{QAM} is given as [12]

$$\begin{aligned} v_{\mathrm{QAM}} &= (1+\eta)^2 \frac{\eta}{1+\eta} \beta + (1+\eta)^2 \frac{\beta}{P} \sigma^2 \\ &= \beta \left[(1+\eta)\, \eta + (1+\eta)^2 \frac{\sigma^2}{P} \right]. \end{aligned} \tag{26}$$

Therefore, the SNR for QAM symbols can be expressed by

$$\gamma_i = \frac{P}{\beta \left[(1+\eta)\, \eta + (1+\eta)^2 \frac{\sigma^2}{P} \right]}. \tag{27}$$

Then, the achievable sum rate is obtained as

$$R = \sum_{i=1}^{K} \log_2(1+\gamma_i). \tag{28}$$

V. Complexity Analysis

The complexity is measured in terms of the required number of floating-point operations per second (flops) [13], [14]. Inversing the $n_k \times n_k$ matrix and the $N_r \times N_t$ matrix requires $4n_k^3/3$ flops and $4N_t^3/3$ flops, respectively, by Gauss–Jordan elimination. The

search for the optimal perturbation vectors within n dimensions requires $O(n^6)$ flops, where $O()$ defines the order of numerical operations [12], and an M-dimensional quadratic programming consumes $O((2M)^3 N)$, where N is the length of the quadratic programming and can be expressed as [11]

$$N = \log_2 (\max |\psi_{i,j}| + 1) + \log_2 (4M) + 1 \tag{29}$$

where $\psi_{i,j}$ is the (i,j)th element of matrix $\mathbf{R}$. With the proposed scheme in this paper, the computational complexity for PSK symbols and QAM symbols are different. Therefore, the complexity for different modulation types must be calculated separately. The total complexity is then obtained as the sum of the complexity of PSK symbols and QAM symbols, which is expressed as

$$\begin{aligned} C &= O\left(4N_t^3/3\right) + O\left(L^6\right) + O\left(8(N_t - L)^3 \cdot N\right) \\ &= O\left(4N_t^3/3\right) + O\left(L^6\right) + O\left(8(N_t - L)^3\right. \\ &\quad \left. \times \left(\log_2 (\max |\psi_{i,j}| + 1) + \log_2 (4M) + 1\right)\right). \end{aligned} \tag{30}$$

VI. Energy Efficiency

To evaluate the usefulness of each VP algorithm, we explore the performance–complexity tradeoff by means of the resulting energy efficiency. Here, the energy efficiency of the proposed JVP is compared with previous VP algorithms in terms of the number of transmit antennas. We define the energy efficiency of the communication link as the bit rate per total transmit power consumed [7], [10], as follows:

$$\mathrm{EE} = \frac{R}{P_{\mathrm{PA}} + N_t \cdot P_0 + p_c \cdot C} \tag{31}$$

where $P_{\mathrm{PA}} = (\xi/\eta - 1)P$ in watts is the power consumed at the power amplifier to produce the total transmit power P of the entire antenna elements and is therefore independent of the number of base station antennas. η is the power amplifier efficiency, and $\xi = 3((\sqrt{M} - 1)/(\sqrt{M} + 1))$ for M-QAM is the modulation-dependent peak-to-average power ratio. $P_0 = P_{\mathrm{mix}} + P_{\mathrm{filt}} + P_{\mathrm{DAC}}$ denotes the power consumption of the mixers and filters and the digital-to-analog converter (DAC), which is regarded as constant in this paper. From [10], the values of each parameter are as follows: $\eta = 0.35$, $P_{\mathrm{mix}} = 30.3$ mW, $P_{\mathrm{filt}} = 2.5$ mW, and $P_{\mathrm{DAC}} = 1.6$ mW, which yields $P_0 = 34.4$ mW. p_c in milliwatts per megaflops denotes the power consumption per 10^6 flops of the digital signal processor. In this paper, we use $p_c = 1/12.8$ mW/Mflops [10].

VII. Numerical Results

Here, we present Monte Carlo simulations of the proposed JCVP, where we assume that $P = 1$; the number of transmit antennas is $N_t = 8$. There are $K = 4$ users, and each is equipped with $n_k = 2$ antennas. The channel error coefficient is assumed as $\alpha = 1$. Except for the conventional VP where all users apply QPSK or 16QAM, it is assumed that users 1, 2 apply QPSK and users 3, 4 apply 16QAM. Above parameters and assumptions remain the same throughout the following simulations. It is intuitive that the benefits of JVP and JCVP extend to other adaptive modulation scenarios.

Fig. 2 shows the bit error rate (BER) performance of two JCVP schemes, where CVP-VP denotes applying CVP first, followed by VP, and VP-CVP denotes applying VP first, followed by CVP. From this figure, it is observed that BD-VP and UG-VP are suboptimal compared with JVP and the proposed JCVP. Moreover, it can be seen that VP-CVP outperforms CVP-VP, and this is because the scaling factor of VP-CVP is smaller than that of CVP-VP by searching the entire constructive areas rather than limited integers. Moreover, the

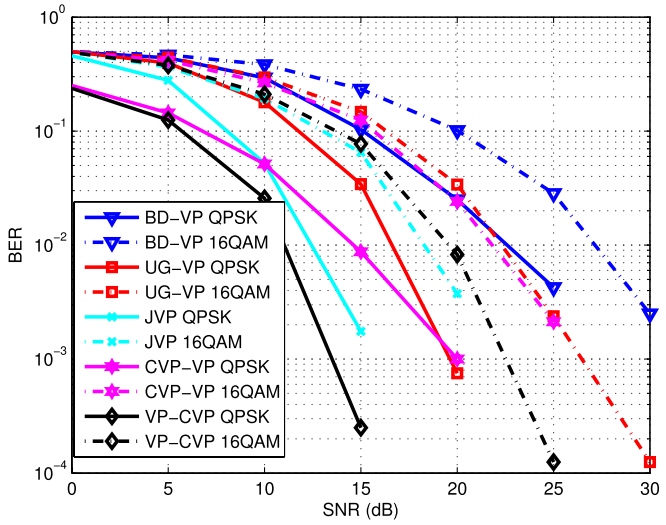

Fig. 2. BER performance of VP schemes, perfect CSI, $N_t = 8$, $K = 4$, and $n_k = 2$.

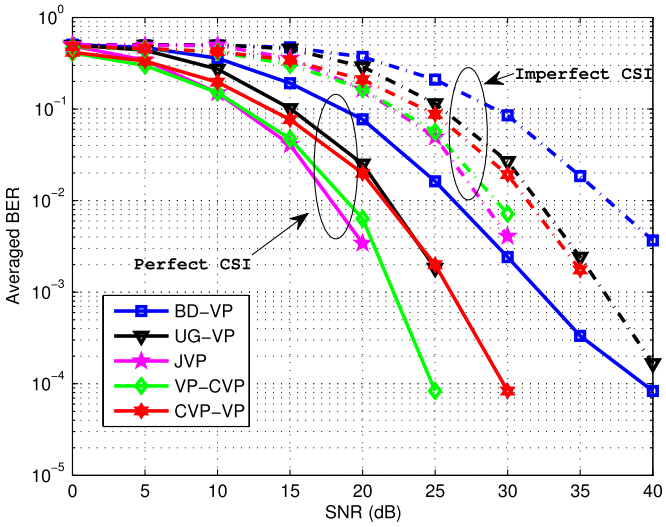

Fig. 3. Average BER performance of different VP schemes, $N_t = 8$, $K = 4$, $n_k = 2$, and $\alpha = 1$.

performance of users applying PSK modulations is better than JVP due to the constructive interference, whereas the users applying QAM modulations suffer a slight performance loss compared with JVP due to the increased value of scaling factor.

Fig. 3 compares the BER performance averaged over all modulations of BD-VP, UG-VP, JVP, VP-CVP, and CVP-VP with perfect CSI and imperfect CSI, respectively. From this figure, a similar BER trend could be seen, and all VP schemes suffer a performance degradation due to the channel estimation error. It is also observed that VP-CVP outperforms CVP-VP in terms of average BER; however, VP-CVP is worse than JVP because JCVP has an inferior performance for users applying QAM modulation.

Fig. 4 shows the computational complexity of different VP schemes, where VP-CVP and CVP-VP are represented by JCVP as they consume the same complexity. It can be seen that, compared with conventional VP and JVP that consume very high complexity, the proposed scheme costs much less complexity while providing a comparable BER performance, which is more significant with the increasing number of antennas. Therefore, it is shown that the proposed scheme could provide a more favorable performance–complexity tradeoff.

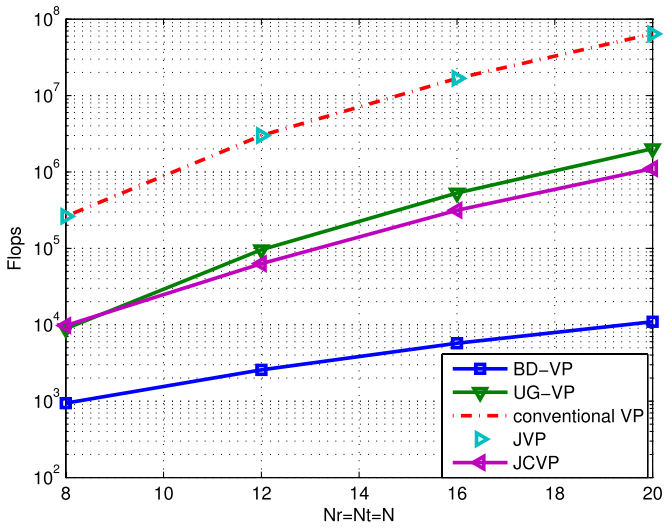

Fig. 4. Computational complexity of different VP schemes. $N_t = N_r$.

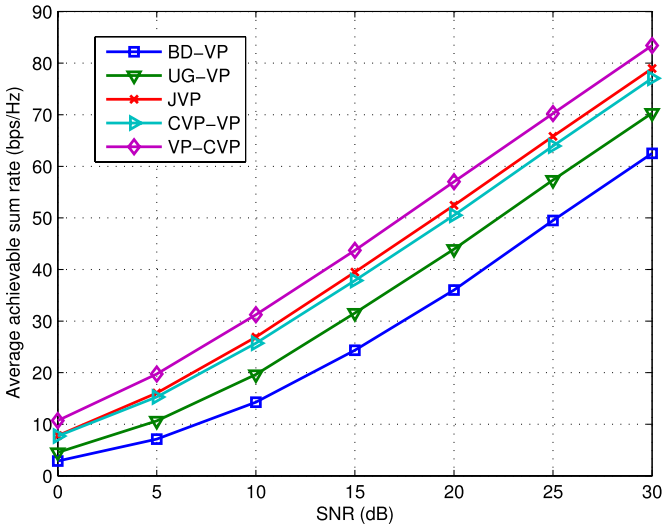

Fig. 5. Achievable sum rate of different VP schemes, $N_t = 8$, $K = 4$, and $n_k = 2$.

Fig. 5 compares the achievable sum rate for different VP schemes. As can be seen from the figure, the proposed VP-CVP offers the largest sum rate, followed by JVP. It is worth noting that, although the scaling factor of VP-CVP is larger than that of JVP, the constructive interference contributes to the sum rate, therefore leading to the superior sum rate performance of VP-CVP. The scaling factor of CVP-VP is large, and the constructive interference could not compensate the noise amplification effect, which leads to a lower sum rate performance.

Fig. 6 shows the energy efficiency for different VP schemes. It is observed that BD-VP and UG-VP have a low energy efficiency performance because of the low sum rate. Moreover, it is seen that CVP-VP has a similar performance to JVP. Although the sum rate of CVP-VP is less than that of JVP, as shown in Fig. 5, CVP-VP consumes less complexity, therefore leading to a similar energy efficiency performance. It is worth noting that VP-CVP achieves the highest energy efficiency, which is due to the superior performance of the sum rate, as illustrated in Fig. 5, and a relatively low complexity in Fig. 4. Therefore, the superior energy efficiency performance of VP-CVP shows that the proposed technique offers a more favorable performance–complexity tradeoff.

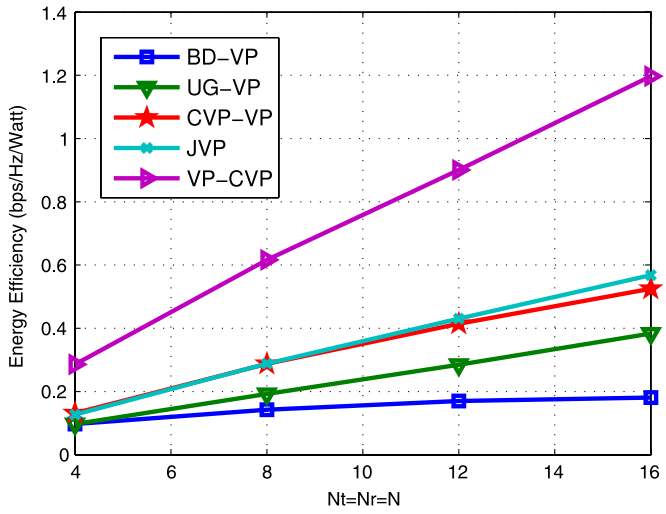

Fig. 6. Energy efficiency of different VP schemes, $N_t = N_r$, $P = 43$ dBm.

VIII. Conclusion

In this paper, a JCVP scheme for multiuser MIMO downlink system that enables the application of VP techniques to adaptive modulation scenarios has been proposed. Furthermore, by limiting the search space to the constructive areas, the perturbation vectors for PSK modulations need not be removed and thus need not be integers. Therefore, a quadratic programming method could instead be applied for symbols from PSK modulations, saving significant computational complexity. Simulation results validate the proposed technique and show that the performance of users applying PSK modulations is much better than that of JVP and the performance of users applying QAM modulations is slightly worse than that of JVP, while the computational complexity is much less, leading to a more favorable performance–complexity tradeoff, which is validated by the energy efficiency performance.

References

[1] *Evolved Universal Terrestrial Radio Access (E-UTRA); Physical Channels and Modulation*, 3GPP TS 36.211, V 8.2.0, Rel. 8, Mar. 2008.

[2] *Evolved Universal Terrestrial Radio Access (E-UTRA):LTE Physical Layer; General Description*, 3GPP TS 36.201, V11.1.0, Rel. 11, Mar. 2008.

[3] M. A. Khojastepour, X. Wang, and M. Madihian, "Design of multiuser downlink linear precoding systems with quantized feedback," *IEEE Trans. Veh. Technol.*, vol. 58, no. 9, pp. 4828–4836, Feb. 2009.

[4] A. Razi, D. J. Ryan, I. B. Collings, and J. Yuan, "Sum rates, rate allocation, and user scheduling for multi-user MIMO vector perturbation precoding," *IEEE Trans. Wireless Commun.*, vol. 9, no. 1, pp. 356–365, Jan. 2010.

[5] C. Masouros, M. Sellathurai, and T. Ratnarajah, "Computationally efficient vector perturbation precoding using thresholded optimization," *IEEE Trans. Commun.*, vol. 61, no. 5, pp. 1880–1890, May 2013.

[6] C. Masouros, M. Sellathurai, and T. Ratnarajah, "A low-complexity sequential encoder for threshold vector perturbation," *IEEE Commun. Lett.*, vol. 17, no. 12, pp. 2225–2228, Dec. 2013.

[7] C. Masouros, M. Sellathurai, and T. Ratnarajah, "Maximizing energy efficiency in the vector precoded MU-MISO downlink by selective perturbation," *IEEE Trans. Wireless Commun.*, vol. 13, no. 9, pp. 4974–4984, Sep. 2014.

[8] C.-B. Chae, S. Shim, and R. W. Heath, "Block diagonalized vector perturbation for multiuser MIMO systems," *IEEE Trans. Wireless Commun.*, vol. 7, no. 11, pp. 4051–4057, Nov. 2008.

[9] R. Chen, C. Li, J. Li, and Y. Zhang, "Low complexity user grouping vector perturbation," *IEEE Wireless Commun. Lett.*, vol. 1, no. 3, pp. 189–192, Jun. 2012.

[10] A. Li and C. Masouros, "A constellation scaling approach to vector perturbation for adaptive modulation in MU-MIMO," *IEEE Wireless Commun. Lett.*, vol. 4, no. 3, pp. 289–292, Jun. 2015.

[11] C. Masouros, M. Sellathurai, and T. Ratnarajah, "Vector perturbation based on symbol scaling for limited feedback MISO downlinks," *IEEE. Trans. Signal Process.*, vol. 62, no. 3, pp. 562–571, Feb. 2014.
[12] J. Maurer, J. Jalden, D. Seethaler, and G. Matz, "Vector perturbation precoding revisited," *IEEE Trans. Signal Process.*, vol. 59, no. 1, pp. 315–328, Jan. 2011.
[13] G. H. Golub and C. F. V. Loan, *Matrix Computations*, 3rd ed. Baltimore, MD, USA: The Johns Hopkins Univ. Press, 1989.
[14] H. Sung, S.-R. Lee, and I. Lee, "Generalized channel inversion methods for multiuser MIMO systems," *IEEE Trans. Commun.*, vol. 57, no. 11, pp. 3489–3499, Nov. 2009.

Transversal Strapdown INS Based on Reference Ellipsoid for Vehicle in the Polar Region

Qian Li, Yueyang Ben, Fei Yu, and Jiubin Tan

***Abstract*—The transversal coordinate system has been proposed to solve the problem of navigation in the Polar Region for a strapdown inertial navigation system (INS). However, it is assumed that the Earth is a perfect sphere in the transversal coordinate system, which is not accurate for a high-precision INS. To solve this problem, we consider the Earth as a reference ellipsoid and then deduct its radii of curvature in our transversal coordinate system. In addition, with the aid of the Bessel geodetic projection method, transformations of navigation quantities from a local-level coordinate system to our transversal coordinate system are derived based on the reference ellipsoid. Numerical results indicate that our method based on the reference ellipsoid performs better than the method based on a reference sphere.**

***Index Terms*—Polar region, reference ellipsoid, strapdown inertial navigation system (INS), transversal coordinate.**

I. Introduction

With the consideration of the self-contained requirement of the Navy protocol and doctrine, a strapdown inertial navigation system (INS), rather than GPS, is strongly recommended for a vehicle in the Polar Region [1]–[5]. However, a local-level coordinate that is usually utilized by an INS is not the best coordinate in the Polar Region because its y-axis always points toward the north. The characteristic of the y-axis results in both mechanical and mathematical difficulties in instrumenting a platform or strapdown attitude matrix [6].

To solve this problem, transversal coordinate system and corresponding navigation algorithm are proposed [7]–[9]. With the concept of the transversal coordinate proposed in [7], we gave the mechanization for a damped transversal strapdown INS in [8] and its system reset method in [9]. In addition, Honeywell Company gave transformations of position and heading angle from a local-level coordinate system to a transversal coordinate system in [10]. Unfortunately, it was assumed in [8]–[10] that the Earth was a perfect sphere in the transversal coordinate system, which was not acceptable for a high-precision INS. Here, we deduct the radiuses of curvature in the transversal coordinate system and develop transformations of navigation quantities based on the reference ellipsoid for a transversal strapdown INS, which would be helpful for decreasing the error brought by the spherical Earth model.

Manuscript received September 27, 2014; revised June 16, 2015; accepted October 24, 2015. Date of publication November 4, 2015; date of current version September 15, 2016. This work was supported by the National Natural Science Foundation of China under Grant 51509063 and Grant 61503090. The review of this paper was coordinated by Prof. T. M. Guerra.

Q. Li and J. Tan are with the Institute of Ultra-precision Optoelectronic Instrument Engineering, Harbin Institute of Technology, Harbin 150001, China (e-mail: liqianheu@163.com).

Y. Ben and F. Yu are with the College of Automation, Harbin Engineering University, Harbin 150001, China (e-mail: byy@hrbeu.edu.cn).

Color versions of one or more of the figures in this paper are available online at http://ieeexplore.ieee.org.

Digital Object Identifier 10.1109/TVT.2015.2497713

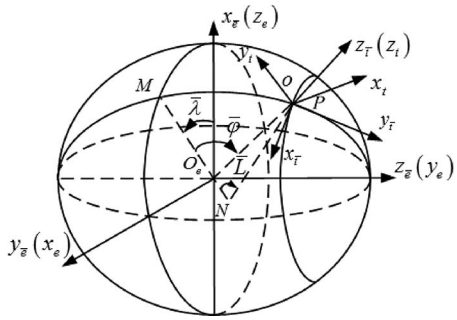

Fig. 1. Coordinate system.

II. Frame Definitions

The China Geodetic Coordinate System 2000 (CGCS-2000) has been adopted as the new national geodetic reference system since July 2008 and is widely used in geodetic technology. Here, we choose it as the reference ellipsoid to complete the design of a transversal strapdown INS. The transversal coordinate system and the local-level coordinate system defined on the reference ellipsoid are shown in Fig. 1.

The local-level coordinate system is an East–North–Up (*E, N, U*) triad. In the transversal coordinate system, the transversal Earth-fixed frame $O_e x_{\bar{e}} y_{\bar{e}} z_{\bar{e}}$ is obtained by revolving $O_e x_e y_e z_e$, which is the Earth-fixed frame in a local-level coordinate system, around two Euler axes successively. In addition, the origin of $O_e x_{\bar{e}} y_{\bar{e}} z_{\bar{e}}$ is at the mass center of the Earth, and the definitions of axes are as follows:

- $O_e x_{\bar{e}}$-axis: pointing toward the North Pole;
- $O_e y_{\bar{e}}$-axis: pointing toward the Greenwich Meridian, lying in the true equatorial plane;
- $O_e z_{\bar{e}}$-axis: 90° east of the Greenwich Meridian, lying in the true equatorial plane.

In Fig. 1, the transversal polar axis is defined as the $O_e z_{\bar{e}}$ axis, whose pointing is defined as transversal north direction. The transversal meridian is defined as the intersecting ellipse of the reference ellipsoid and a plane passing through the $O_e z_{\bar{e}}$ axis, and the transversal meridian passing through point $x_{\bar{e}}$ is transversal Greenwich Meridian. The transversal latitude line is defined as the intersecting circle of the reference ellipsoid and a plane perpendicular to the $O_e z_{\bar{e}}$ axis, and the transversal latitude line passing through point $x_{\bar{e}}$ is treated as the transversal equator. M is the intersecting point of the transversal equator and the transversal meridian passing through point P, which represents the position of a vehicle.

The position P can be determined by transversal longitude $\bar{\lambda}$ and transversal geographic latitude $\bar{L}$ (represented by transversal latitude in the sequel). To compare with [8]–[10], transversal geocentric latitude $\bar{\varphi}$ is also introduced here. The definitions of transversal longitude and transversal geocentric latitude have been given in [8]–[10]. The transversal latitude is the angle between the transversal equatorial plane and NP, which is normal to the reference ellipsoid at point P. Note that point N is the intersecting point of the normal at point P and the transversal equatorial plane.